crystals

MDPI

Article

Thermal Stability of the Ultra-Fine-Grained Structure and Mechanical Properties of AlSi7MgCu0.5 Alloy Processed by Equal Channel Angular Pressing at Room Temperature

Miloš Matvija [1,*], Martin Fujda [1], Ondrej Milkovič [2,3], Marek Vojtko [2] and Katarína Gáborová [1]

[1] Institute of Materials, Faculty of Materials, Metallurgy and Recycling, Technical University of Košice, Letná 1/9, 042 00 Košice, Slovakia; martin.fujda@tuke.sk (M.F.); katarina.gaborova@tuke.sk (K.G.)
[2] Institute of Materials Research, Slovak Academy of Sciences, Watsonova 47, 040 01 Košice, Slovakia; omilkovic@saske.sk (O.M.); mvojtko@saske.sk (M.V.)
[3] Institute of Experimental Physics, Slovak Academy of Sciences, Watsonova 47, 040 01 Košice, Slovakia
* Correspondence: milos.matvija@tuke.sk; Tel.: +421-55-602-2539

Abstract

Understanding the limitations of cold-formed aluminum alloys in practice applications is essential, particularly due to the risk of substructural changes and a reduction in strength when exposed to elevated temperatures. In this study, the thermal stability of the ultra-fine-grained (UFG) structure formed by equal channel angular pressing (ECAP) at room temperature and the mechanical properties of the AlSi7MgCu0.5 alloy were investigated. Prior to ECAP, the plasticity of the as-cast alloy was enhanced by a heat treatment consisting of solution annealing, quenching, and artificial aging to achieve an overaged state. Four repetitive passes via ECAP route A resulted in the homogenization of eutectic Si particles within the α-solid solution, the formation of ultra-fine grains and/or subgrains with high dislocation density, and a significant improvement in alloy strength due to strain hardening. The main objective of this work was to assess the microstructural and mechanical stability of the alloy after post-ECAP annealing in the temperature range of 373–573 K. The UFG microstructure was found to be thermally stable up to 523 K, above which notable grain and/or subgrain coarsening occurred as a result of discontinuous recrystallization of the solid solution. Mechanical properties remained stable up to 423 K; above this temperature, a considerable decrease in strength and a simultaneous increase in ductility were observed. Synchrotron radiation X-ray diffraction (XRD) was employed to analyze the phase composition and crystallographic characteristics, while transmission electron microscopy (TEM) was used to investigate substructural evolution. Mechanical properties were evaluated through tensile testing, impact toughness testing, and hardness measurements.

Keywords: aluminum alloy; equal channel angular pressing; heat treatment; microstructure; mechanical properties; phase analyses; thermal stability

check for updates

Academic Editor: Jinfeng Nie

Received: 6 July 2025
Revised: 20 July 2025
Accepted: 28 July 2025
Published: 31 July 2025

Citation: Matvija, M.; Fujda, M.; Milkovič, O.; Vojtko, M.; Gáborová, K. Thermal Stability of the Ultra-Fine-Grained Structure and Mechanical Properties of AlSi7MgCu0.5 Alloy Processed by Equal Channel Angular Pressing at Room Temperature. *Crystals* **2025**, *15*, 701. https://doi.org/10.3390/cryst15080701

Copyright: © 2025 by the authors. Licensee MDPI, Basel, Switzerland. This article is an open access article distributed under the terms and conditions of the Creative Commons Attribution (CC BY) license (https://creativecommons.org/licenses/by/4.0/).

1. Introduction

Research on foundry aluminum alloys, particularly precipitation-hardenable Al–Si–Mg–Cu-type alloys, has led to many innovations in the commercial production of castings, especially in the automotive and aerospace industries. The specific properties of these alloys with varying Mg and Cu contents continue to enable novel application opportunities [1–3]. In recent years, the concept of plastically deforming alloys originally developed for casting

has gained increasing attention, thus expanding their potential use in metal-forming technologies. The limited plasticity of cast states, due to the casting structure, presence of intermetallic phases, and casting defects, significantly restricts their deformability. One possible approach is deformation at elevated temperatures; however, this often results in undesirable dynamic recovery and recrystallization. Therefore, deformation at room temperature is preferred, as it prevents softening processes and enables the development of fine-grained microstructures.

The ECAP (equal channel angular pressing) technique, originally proposed by V. M. Segal [4], is one of the most effective severe plastic deformation (SPD) methods, allowing for substantial grain refinement and structural homogenization. The mechanism of shear deformation in polycrystalline materials is influenced by grain or subgrain boundaries and their misorientation, which serve as barriers to dislocation movement. The strengthening contribution of a fine-grained structure is described by the Hall–Petch relationship [5,6]. The increase in the strength of deformed materials results from the superposition of several strengthening mechanisms: Peierls–Nabarro stress, dislocation strengthening, solid solution strengthening, precipitation strengthening, and grain/subgrain boundary strengthening.

Since complex-shaped castings made from these alloys cannot be plastically deformed without altering their geometry, their direct application in SPD processes is limited. However, Al–Si–Mg–Cu alloys in the form of semi-finished products enable the use of ECAP to achieve ultra-fine-grained (UFG) structures with grain sizes below 1 μm, resulting in significantly improved mechanical properties—particularly strength, toughness, and, in certain cases, superplasticity [7–9].

Aluminum alloys are well suited for ECAP processing due to their good plasticity at both room and elevated temperatures, low deformation resistance, and favorable shear deformability. Numerous studies have investigated the effects of ECAP on the microstructural evolution of foundry aluminum alloys, including different processing routes [10,11], as well as microstructural, substructural, and mechanical property changes at elevated temperatures where deformation resistance is lower [12–15] and at room temperature where solid solution strengthening is more pronounced [16–19]. Furthermore, authors [20–23] examined the influence of prior heat treatment combined with subsequent ECAP processing on the resulting microstructure and mechanical properties, demonstrating that varying property levels can be achieved depending on the specific alloy used.

In [23], the processing of commercial Al–Si–Mg–Cu foundry alloys by ECAP at room temperature is described in detail, aiming to achieve the highest possible degree of severe plastic deformation without inducing material failure. As the successful application of this technique requires sufficient plasticity of the base material, a prior heat treatment is essential to enhance the ductility of the originally brittle as-cast structures.

The impact of ECAP processing on the microstructure and mechanical properties of aluminum alloys is well documented. However, it is also necessary to investigate the changes that occur during service, particularly under elevated temperature conditions. The microstructural and mechanical improvements induced by ECAP are thermally stable only up to a certain temperature. Beyond this threshold, recovery and recrystallization processes, grain coarsening, and a decrease in strength properties take place, which significantly limit the practical applicability of such processed alloys.

The scientific contribution of this work lies in determining the thermal stability of the ultra-fine-grained structure of the AlSi7MgCu0.5 alloy based on a detailed analysis of grain and subgrain morphology within the α-solid solution, as well as phase composition analysis. Additionally, the stability of the alloy's mechanical properties is assessed, which is essential from the perspective of potential applications.

2. Materials and Methods

2.1. Experimental Material

A commercial, heat-treatable, hypoeutectic AlSi7MgCu0.5 foundry alloy, with its chemical composition listed in Table 1, was used for the investigation.

Table 1. Chemical composition of AlSi7MgCu0.5 alloy [23].

Element	Si	Cu	Mg	Fe	Ti	Mn	Sr	Zn	Al
wt.%	6.49	0.45	0.38	0.11	0.11	0.08	0.03	0.01	Bal.

The as-cast state of the alloy served as the initial condition for the experiments. The casting was produced using gravity die casting technology under optimized mold cooling conditions. Prior to casting, the molten AlSi7MgCu0.5 alloy was modified with strontium and inoculated using an Al–Ti–B grain refiner to optimize the resulting microstructure.

2.2. Material Processing

The processing of the as-cast alloy consisted of (i) heat treatment prior to severe plastic deformation (SPD) by equal channel angular pressing (pre-ECAP heat treatment), (ii) severe plastic deformation by ECAP at room temperature, and (iii) heat treatment after ECAP (post-ECAP annealing).

The pre-ECAP heat treatment was carried out to increase the alloy's plasticity with the aim of maximizing its mechanical properties after SPD. The optimized heat treatment consisted of solution annealing, followed by artificial aging to achieve the overaged state of the alloy. The solution annealing of the alloy was performed at 823 K for 4 h, followed by water quenching at 298 K and artificial aging at 573 K for 5 h, with subsequent air cooling. For optimal pre-ECAP heat treatment and subsequent forming by the ECAP technique, cylindrical samples with a diameter of Ø = 10 mm and a length of l_0 = 100 mm were prepared from the alloy.

After heat treatment, the samples were deformed to multiple passes through the ECAP die with channel angles of Φ = 90° and Ψ = 37° (Figure 1) at room temperature. The total number of ECAP passes was N = 4. The pressing was realized using route A, without rotating the samples between consecutive ECAP passes. The pressing rate through the ECAP die was 100 mm·min^{-1} for the first two passes and 50 mm·min^{-1} for the remaining two passes. ECAP processing was realized to produce an ultra-fine-grained (UFG) structure and to homogenize the alloy microstructure. The orientation and designation of the X, Y, and Z planes of the pressed samples were defined as shown in Figure 1.

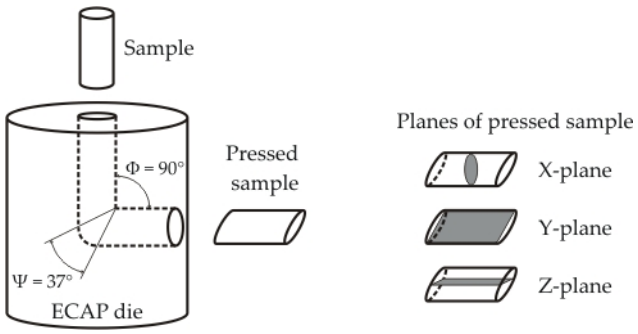


Figure 1. Schematic representation of the ECAP technique and the designation of planes in the pressed sample [23].

After ECAP processing, the alloy samples were post-ECAP-annealed at temperatures of 373, 423, 473, 523, and 573 K for 2 h, followed by air cooling. Post-ECAP annealing was

carried out to evaluate the thermal stability of the UFG structure formed during SPD and the thermal stability of the resulting mechanical properties. A temperature–time diagram of processes is given in Figure 2.

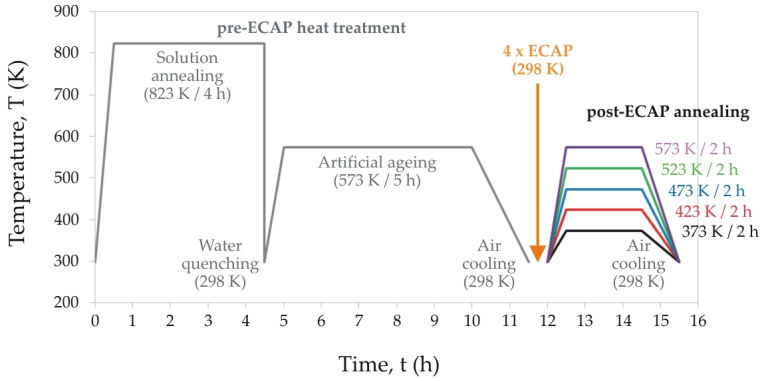


Figure 2. Schematic temperature–time diagram of processes.

2.3. Experimental Setup

The microstructure of the analyzed alloy was documented in the as-cast state, after pre-ECAP heat treatment, following ECAP processing, and after post-ECAP annealing. Light microscopy (LM) was performed using an Olympus Vanox-T microscope, and scanning electron microscopy (SEM) with secondary electron (SE) detection was performed using a JEOL 7000F microscope, which was also used for energy dispersive X-ray (EDX) analysis of individual phases present in the alloy microstructure. Metallographic samples were prepared using standard metallographic techniques, including cold mounting in resin, grinding, polishing, and etching with a solution of 0.5% HF in distilled water. Substructure analysis of the alloy using thin foils was performed using a transmission electron microscope (TEM) JEOL JEM-2000FX. Thin foils were electrolytically prepared using a Struers TenuPol-5 at a temperature of 238 K and a voltage of 16 V. The electrolyte consisted of 33% HNO_3 and 67% CH_3OH. The average size (width and length) of grains and/or subgrains present in the substructure of the analyzed alloys was determined based on a 200 measurements per alloy condition using statistical metallographic methods.

Phase analysis of the experimental alloy structures was performed using high-energy X-ray diffraction performed in transmission mode at the experimental hutch P02.1 Powder Diffraction and Total Scattering Undulator Beamline [24] at the PETRA III synchrotron source (a third-generation synchrotron source) [25] at DESY in Hamburg. At the P02.1 hutch, cylindrical samples (Ø = 10 mm, l = 4 mm) were irradiated for 20 s with a photon beam of 58 keV energy and a wavelength of λ = 0.207271 Å, using a beam cross section of 0.5 × 0.5 mm. The X-ray beam irradiated the sample in the direction of the longitudinal axis, and the diffraction patterns were recorded using a fast 2D Perkin Elmer XRD 1621 detector with 2048 × 2048 pixels and a pixel size of 200 µm × 200 µm [26]. The sample-to-detector distance, orthogonal alignment of the detector with respect to the photon beam, detector center position, and photon energy were calibrated using a CeO_2 reference sample. During the in situ diffraction measurements (post-ECAP annealing), the samples were placed inside a Linkam THMS600 heating stage under an argon inert atmosphere [27], with a controlled heating rate of 20 K·min^{-1}. The resulting images were integrated into intensity vs. 2Θ angle plots using the FIT2D software [28]. The average sizes (width and length) of grains and subgrains present in the substructure of the analyzed alloys were determined using statistical metallographic methods.

Hardness measurements were carried out using the Vickers method [29] on polished specimen surfaces at room temperature. Hardness measurements were carried out with

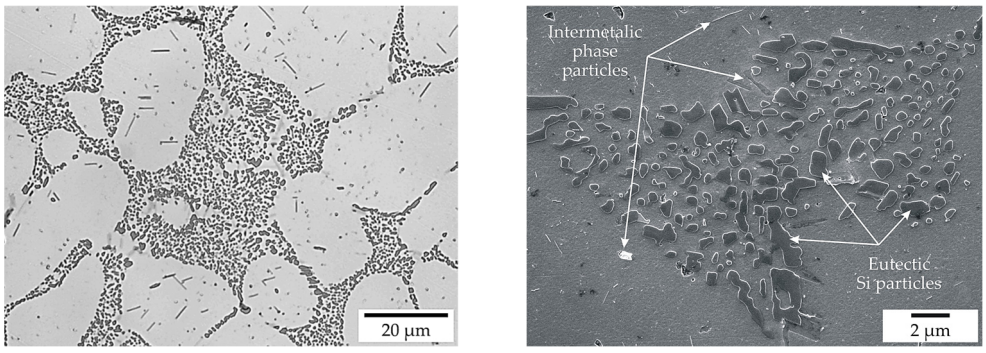
10 indentations per sample in areas with a complex microstructure, including α-solid solution, eutectic regions, and intermetallic phase particles. Vickers microhardness (HV0.2) was assessed with an Anton Paar MHT-4 microhardness tester and an Olympus Vanox-T light microscope. The strength properties and ductility characteristics of analyzed AlSi7MgCu0.5 alloy states were evaluated by tensile testing [30] using a Hegewald & Peschke Zwick 1387 universal testing machine. The tests were performed on short cylindrical samples with dimensions d_0 = 5 mm and l_0 = 10 mm at a strain rate of 2.5 × 10^{-4} s^{-1} and at room temperature. The evaluated strength parameters included the 0.2% offset yield strength ($Rp_{0.2}$) and ultimate tensile strength (Rm), while ductility parameters included the plastic elongation at maximum load (Ag), total elongation (A), and reduction of area (Z). The impact toughness of selected alloy states was determined by Charpy impact testing [31] in a three-point bending configuration using a PS 30 pendulum impact tester. The test was carried out on non-standard samples with dimensions 8 × 4 × 55 mm, containing a U-notch with a depth of 2 mm and a width of 1 mm, tested at room temperature. The impact toughness (KCU) was calculated as the ratio of the impact energy (KU, in J) required to fracture the sample to the initial cross-sectional area under the notch (S_0, in cm^2). The impact test was performed at the threshold temperature at which the ultra-fine-grained structure of the alloy remained stable.

3. Results

3.1. Microstructure, Substructure, and Phase Analysis

3.1.1. Microstructure and Substructure of AlSi7MgCu0.5 Alloy

The microstructure of the AlSi7MgCu0.5 alloy in the as-cast state was heterogeneous and dendritic. It consisted of a primary α-solid solution, eutectic regions composed of α + Si, and intermetallic phase particles, as illustrated in Figure 3a,b. The eutectic Si particles exhibited a fine globular and rod-like morphology in the center of the eutectic cells and a coarser rod-like morphology near the α-solid solution dendrites. Within the α-solid solution, needle-shaped particles based on Cu, Mg, Si, and Al were observed; according to the EDX analysis, these are likely Q-phase particles (Q-$Al_4Mg_8Si_7Cu_2$) (Figure 4a), along with needle- or rod-like particles composed of Si (Figure 4b). Intermetallic phase particles of a rod-like morphology located at the interface between the α-solid solution and eutectic regions, containing Fe, Mn, Mg, Cu, and Al, were identified by EDX analysis as $Al_x(Fe,Mn)_ySi_z$ silicides with Mg and Cu content (Figure 4c). Plate-like particles with Cu, Mg, Si, and Al content were also present and can be considered as the Q-phase (Q-$Al_4Mg_8Si_7Cu_2$) (Figure 4d).



(**a**) (**b**)

Figure 3. Microstructure of the as-cast AlSi7MgCu0.5 alloy documented after chemical etching using: (**a**) light microscopy (LM) and (**b**) scanning electron microscopy (SEM).

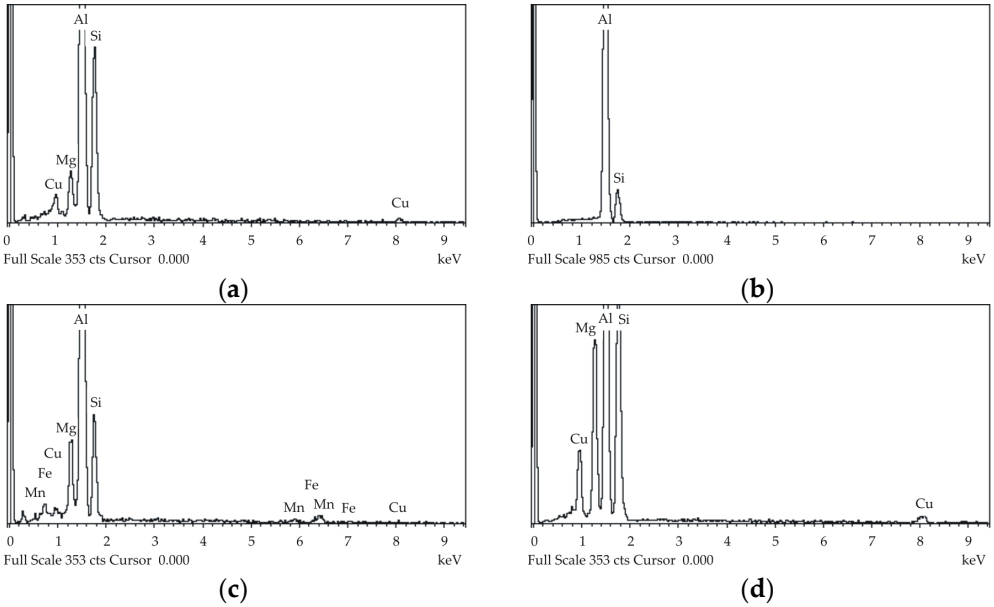


Figure 4. EDX spectra of intermetallic phase particles in the as-cast state of the alloy: (**a**) needle-like morphology composed of Cu, Mg, Si, and Al (identified as Q-$Al_4Mg_8Si_7Cu_2$); (**b**) needle-like and rod-like morphology composed primarily of Si; (**c**) rod-like morphology located at the interface between the α-solid solution and eutectic Si particles, composed of Fe, Mn, Mg, Cu, and Al (identified as $Al_x(Fe,Mn)_ySi_z$ silicide); and (**d**) plate-like morphology composed of Cu, Mg, Si, and Al (identified as Q-$Al_4Mg_8Si_7Cu_2$).

The optimization of the pre-ECAP heat treatment of the AlSi7MgCu0.5 alloy involved determining the solution annealing and artificial aging conditions to achieve the overaged state of the alloy. This was performed with the aim of increasing the alloy's plasticity prior to ECAP processing at room temperature. Figure 5a,b shows the microstructure of the AlSi7MgCu0.5 alloy after optimized solution annealing at 823 K for 4 h, followed by water quenching. A comparison with the as-cast microstructure (Figure 3a,b) clearly indicates that the solution annealing process led primarily to a pronounced spheroidization and coarsening of the eutectic Si particles. During solution annealing at 823 K, dissolution of Q-$Al_4Mg_8Si_7Cu_2$ intermetallic phase particles and morphological modification of the $Al_x(Fe,Mn)_ySi_z$ intermetallic phase were also observed, as confirmed by the EDX analysis of intermetallic particles present in the alloy microstructure (Figure 6a,b).

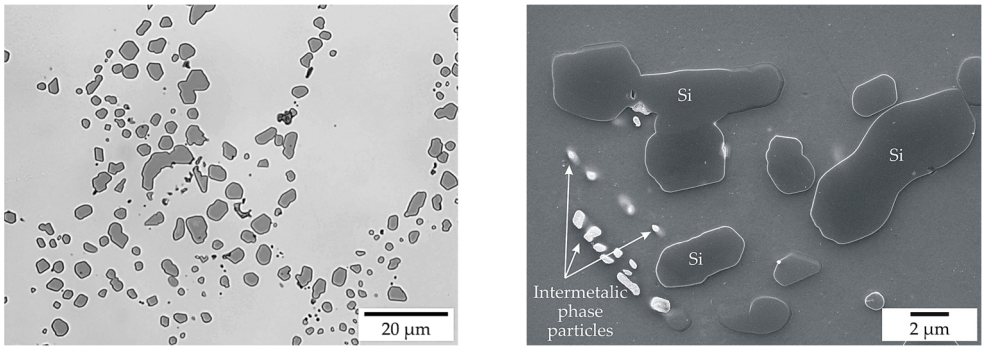
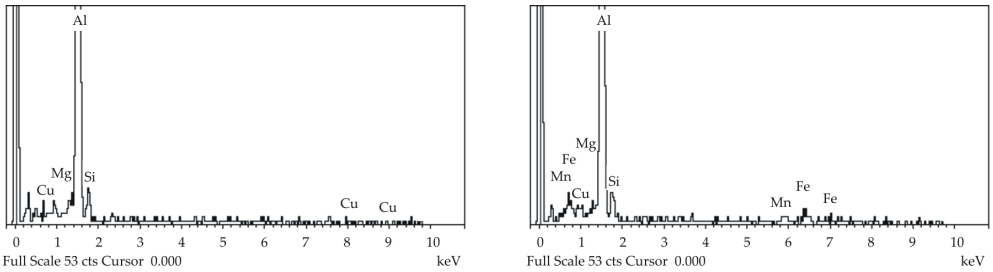


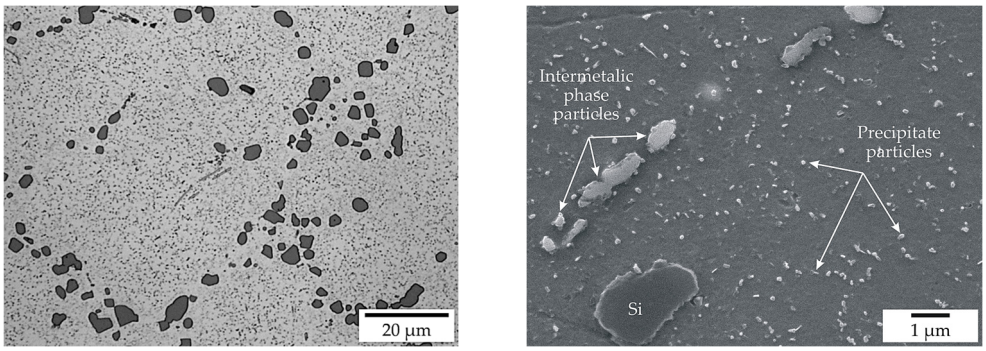
Figure 5. Microstructure of solution-annealed AlSi7MgCu0.5 alloy documented after chemical etching using (**a**) light microscopy (LM) and (**b**) scanning electron microscopy (SEM).



(**a**) (**b**)

Figure 6. EDX spectra of intermetallic phase particles in the solution-annealed state of the alloy: (**a**) globular morphology composed of Cu, Mg, Si, and Al (identified as Q-$Al_4Mg_8Si_7Cu_2$) and (**b**) rod-like morphology located at the interface between the α-solid solution and eutectic Si particles, composed of Fe, Mn, Mg, Cu, and Al (identified as $Al_x(Fe,Mn)_ySi_z$ silicide).

The optimized artificial aging consisted of annealing at 573 K for 5 h, during which a significant increase in the plasticity of the investigated alloy was achieved. This pre-ECAP heat treatment resulted in a twofold increase in alloy toughness compared with the as-cast alloy state. The microstructure of the AlSi7MgCu0.5 alloy in the overaged state is shown in Figure 7a,b. During artificial aging, fine incoherent precipitates formed from the supersaturated solid solution. These precipitates exhibited globular, oval, and rod-like morphologies and were uniformly distributed throughout the α-solid solution. The precipitate particles documented using transmission electron microscopy are shown in Figure 8a. According to the EDX analysis, they contained Mg and Si—likely corresponding to the β-phase (Mg_2Si) (Figure 8b); Cu, Mg, Si, and Al—likely corresponding to the Q-phase ($Al_4Mg_8Si_7Cu_2$) (Figure 8c); and Si particles in the α-solid solution (Figure 8d).



(**a**) (**b**)

Figure 7. Microstructure of overaged AlSi7MgCu0.5 alloy documented after chemical etching using (**a**) light microscopy (LM) and (**b**) scanning electron microscopy (SEM).

Severe plastic deformation by the ECAP technique at room temperature significantly influenced the microstructure and substructure of the AlSi7MgCu0.5 alloy. The samples were pressed four times through the ECAP die channel without rotation between passes (route A). This processing after the application of pre-ECAP heat treatment resulted in the effective elimination of the heterogeneous dendritic structure through fragmentation and redistribution of eutectic Si particles, intermetallic phase particles, and precipitated particles from the solid solution in the analyzed alloy.

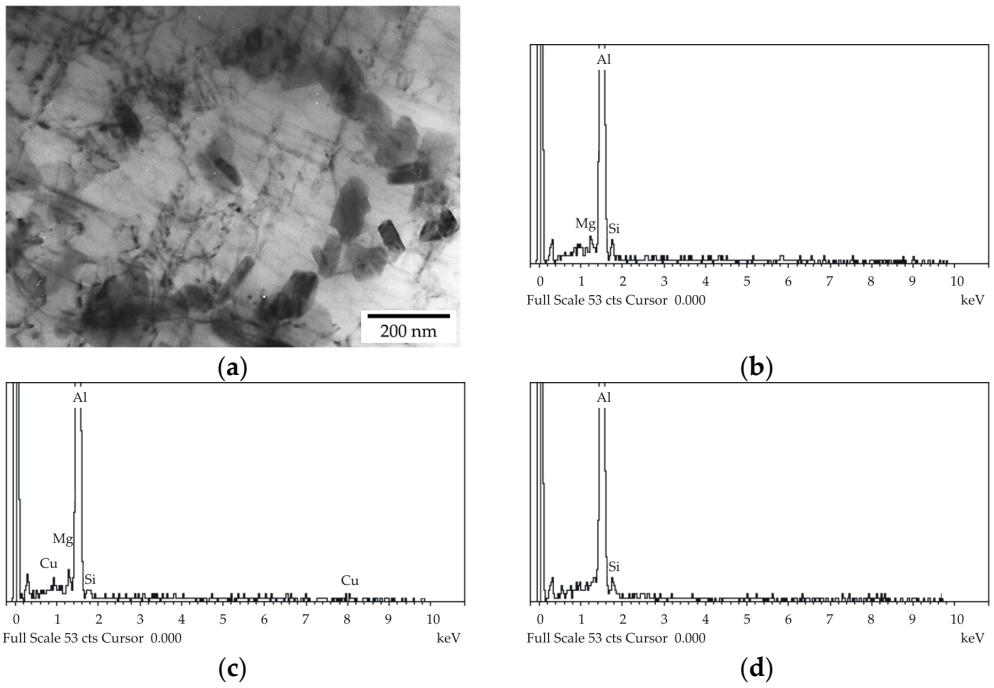


Figure 8. (**a**) Incoherent precipitates formed from the supersaturated solid solution during artificial aging (TEM) and EDX spectra of incoherent precipitates in the overaged state of the alloy showing (**b**) Mg and Si (corresponding to the β-Mg_2Si phase); (**c**) Cu, Mg, Si, and Al (corresponding to the Q-phase, $Al_4Mg_8Si_7Cu_2$); and (**d**) Si particles.

The microstructure in the X, Y, and Z planes of the ECAP-processed AlSi7MgCu0.5 alloy is shown in Figure 9a–c. A comparison of the microstructures after ECAP with pre-ECAP heat-treated state clearly reveals the homogenization of the alloy structure and the rearrangement of eutectic Si particles within the α-solid solution. The application of the ECAP technique did not alter the morphology of the eutectic Si particles; however, their previously non-uniform distribution in the α-matrix transformed into a band-like arrangement in the X and Y planes of the samples. In the Z plane, the homogenization effect was less pronounced, which can be attributed to the deformation of the cubic element of the pressed samples due to the nature of ECAP processing route A. The application of the ECAP technique resulted in the formation of an ultra-fine-grained structure in the alloy, as evidenced by the substructures documented by transmission electron microscopy in the X and Y planes and by the formation of a cellular substructure in the Z plane (Figure 9d–f). The ECAP processing of the AlSi7MgCu0.5 alloy at room temperature led to the development of a cellular dislocation substructure and the formation of fine elongated grains or subgrains with a high dislocation density, predominantly separated by wavy, unstable boundaries. The grains and/or subgrains were separated by both high-angle and low-angle boundaries, exhibiting a significant degree of preferential structural orientation, as confirmed by the results of selected area electron diffraction (SAED) analysis performed on the alloy sample.

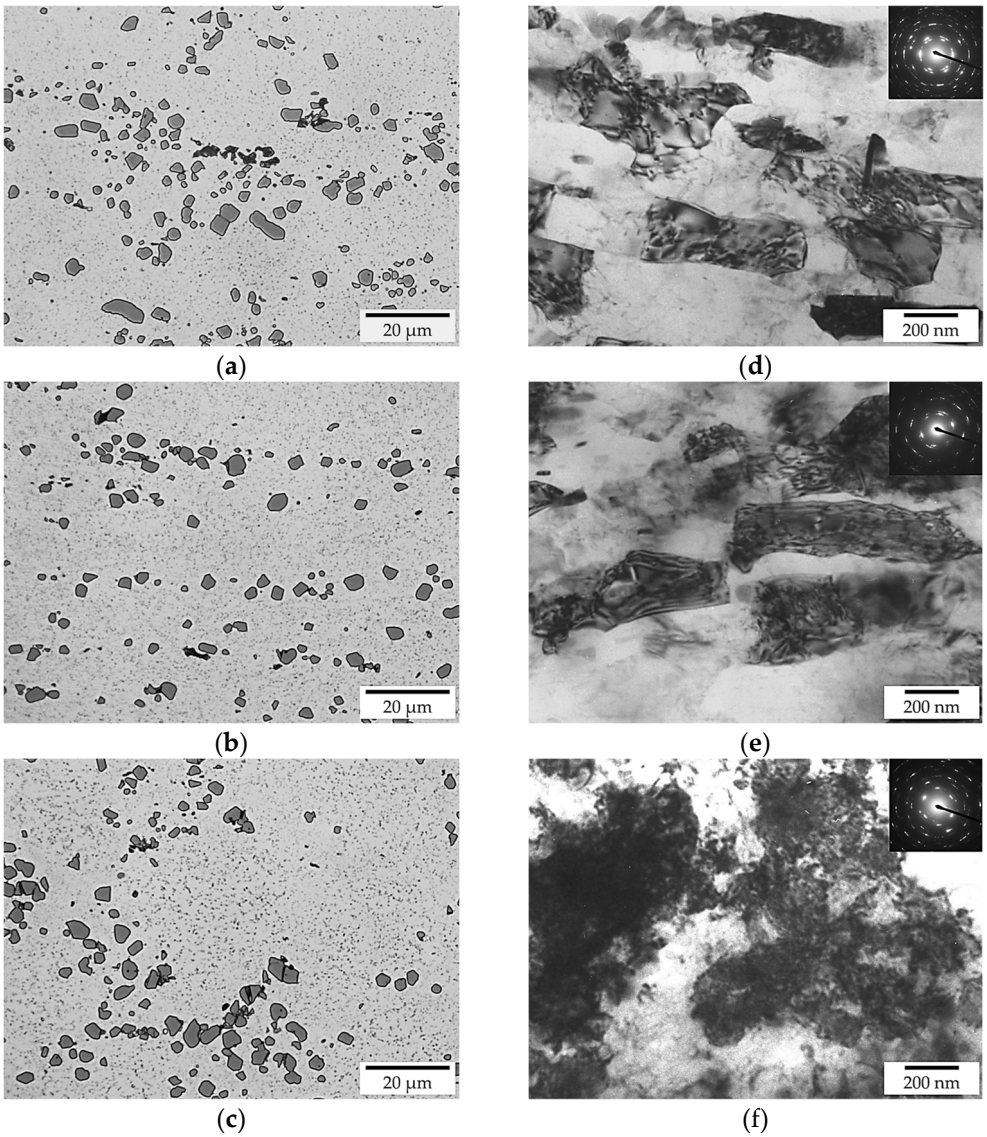


Figure 9. Microstructure of ECAP-processed AlSi7MgCu0.5 alloy documented after chemical etching using light microscopy (LM) in (**a**) the X plane, (**b**) Y plane, and (**c**) Z plane of pressed sample and transmission electron microscopy (TEM) in (**d**) the X plane, (**e**) Y plane, and (**f**) Z plane of pressed sample with the diffraction patterns from selected area electron diffraction (SAED).

After SPD of the analyzed alloy, post-ECAP annealing was carried out to determine the thermal stability of the UFG structure formed during four passes of the alloy samples through the ECAP die at room temperature. Figure 10 shows the microstructures of the AlSi7MgCu0.5 alloy in the post-ECAP-annealed state at temperatures of 373–573 K for 2 h in the X plane of the pressed samples. Post-ECAP annealing within the temperature range of 373–573 K had no significant effect on the microstructure of the alloys (i.e., morphology and distribution of eutectic Si particles, intermetallic phase particles, and precipitates), as evident when compared with the ECAP-processed microstructure. However, significant changes occurred in the substructure of the α-solid solution.

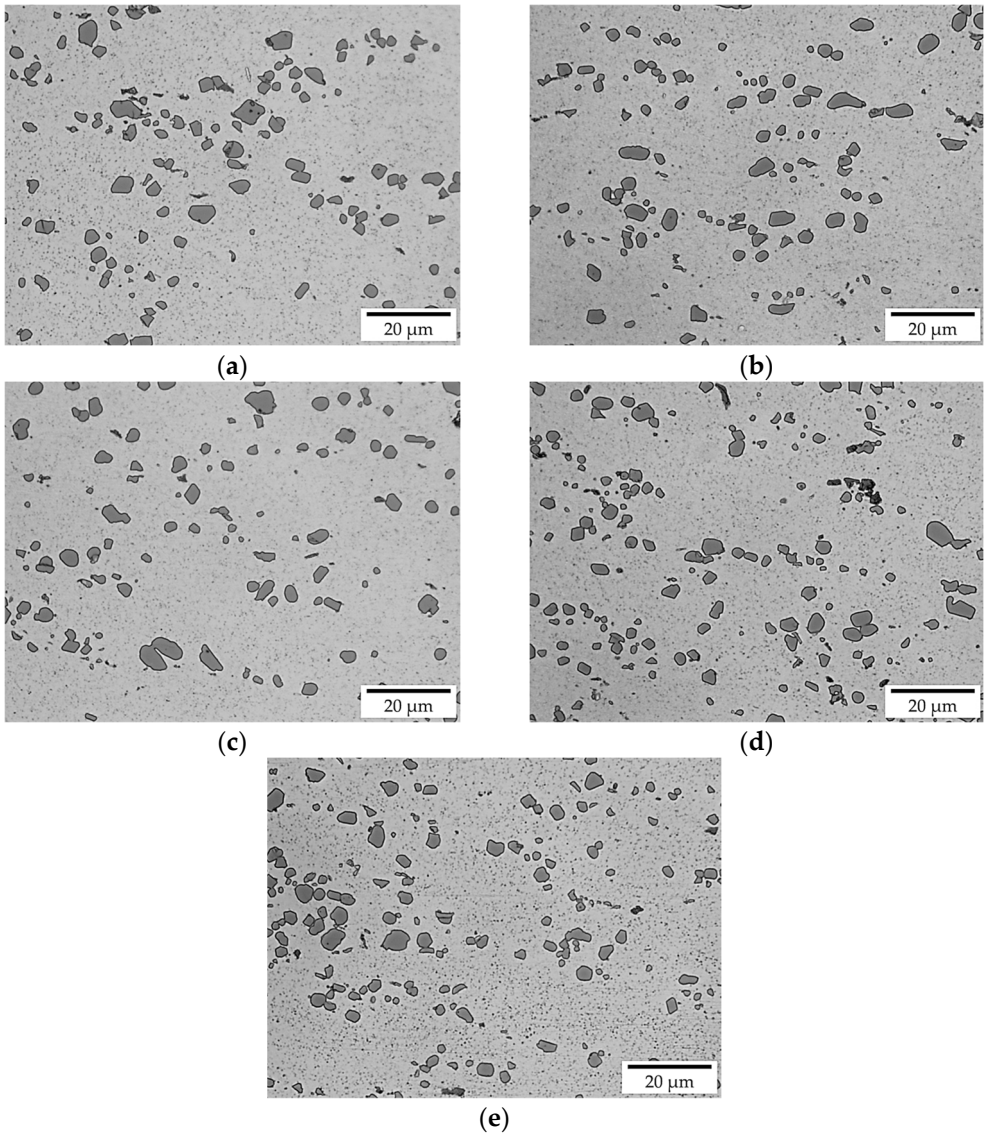


Figure 10. Microstructure of post-ECAP-annealed AlSi7MgCu0.5 alloy documented after chemical etching using light microscopy (LM) in the X plane of pressed sample after annealing at (**a**) 373 K, (**b**) 425 K, (**c**) 473 K, (**d**) 523 K, and (**e**) 573 K for 2 h.

The increasing temperature of post-ECAP annealing led to a gradual growth of the elongated deformed grains or subgrains of the α-solid solution in the analyzed alloy, accompanied by a reduction in dislocation density. The substructure of the AlSi7MgCu0.5 alloy after post-ECAP annealing at 373 K for 2 h is shown in Figure 11a. Annealing resulted in a slight increase in the average grain and/or subgrain length in the analyzed X plane compared with the ECAP-processed state of the alloy, while the average width remained unchanged (Table 2). The grains and/or subgrains exhibited the same characteristics as those observed in the ECAP-processed state—they had a rounded shape and high dislocation density and were separated by both low-angle and high-angle boundaries, as illustrated by the diffraction pattern in Figure 11a. Annealing at 423 K resulted in a more pronounced increase in the average width and length of the deformed grains and/or subgrains of the AlSi7MgCu0.5 alloy solid solution, along with a slight reduction in dislocation density (Figure 11b), in comparison with the ECAP-processed state. The subgrains exhibited wavy, non-equilibrium boundaries with both high-angle and low-angle misorientations, as confirmed by diffraction analysis. In the case of post-ECAP annealing at 473 K, the average grain and/or subgrain width increased to 310 nm, and the length

reached 900 nm. The substructure shown in Figure 11c reveals a reduction in dislocation density. The grains and/or subgrains exhibited rounded boundaries, and according to the diffraction pattern, both low-angle and high-angle misorientations were present. Annealing at 523 K led to recovery of the substructure of the solid solution. Figure 11d shows areas where partial straightening of grain boundaries and a decrease in dislocation density occurred, as well as regions where grains and/or subgrains still exhibited an elongated shape. Diffraction analysis indicated the presence of both low-angle and high-angle grain and/or subgrain boundaries within the substructure.

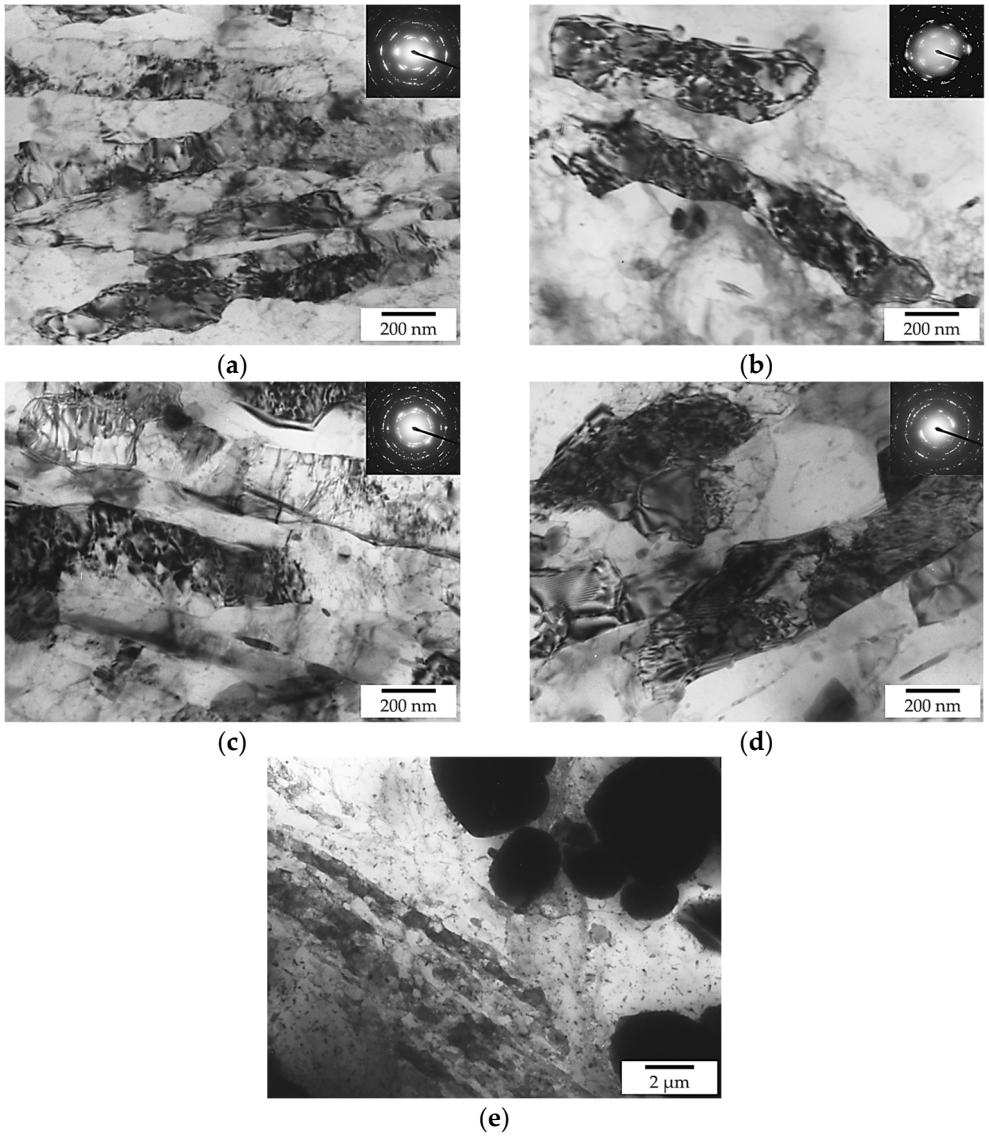


Figure 11. Substructure of post-ECAP-annealed AlSi7MgCu0.5 alloy documented using transmission electron microscopy (TEM) in the X plane of pressed sample after annealing at (**a**) 373 K, (**b**) 425 K, (**c**) 473 K, (**d**) 523 K, and (**e**) 573 K for 2 h.

Post-ECAP annealing at 573 K resulted in the local formation of equiaxed grains with relatively straight boundaries in regions adjacent to eutectic Si particles, with an average grain size of 4.8 μm. In areas farther from these regions, elongated grains and/or subgrains were present, with an average width of 550 nm and length of 1.6 μm (Figure 11e). Diffraction patterns confirmed that the structure was predominantly composed of grains with high-angle boundaries.

Table 2. Grain and/or subgrain size of α-solid solution of AlSi7MgCu0.5 alloy in the X plane after ECAP processing and post-ECAP annealing.

Alloy State	Average Width (nm)	Average Length (nm)
ECAP-processed [23]	200	650
Post-ECAP-annealed at 373 K	200	730
Post-ECAP-annealed at 423 K	290	900
Post-ECAP-annealed at 473 K	310	900
Post-ECAP-annealed at 523 K	330	960
Post-ECAP-annealed at 573 K	550	1600

An increase in post-ECAP annealing temperature led to a gradual growth of the grain and/or subgrain size within the solid solution. Evaluation of the average grain and/or subgrain size indicated that the alloy retained its UFG structure up to 523 K. The difference between the average width and length of grains and/or subgrains increased with rising annealing temperature, with the largest discrepancy observed at 573 K. As shown in Table 2, the increase in grain and/or subgrain length was more pronounced than the increase in their width. The annealing temperature of 523 K can be considered a threshold or critical temperature, above which significant grain growth occurs due to partial recrystallization of the solid solution.

According to previous studies [23] that form the basis of this research, it is evident that the microstructure of the alloy after the application of the ECAP technique consisted of grains and/or subgrains bounded by both high-angle and low-angle grain boundaries. The grain and/or subgrain size distribution was heterogeneous due to the presence of eutectic Si particles. Broader bands composed of elongated subgrains with low-angle boundaries were observed in regions farther from these eutectic Si particles, as documented and analyzed by TEM. In contrast, finer equiaxed grains with high-angle grain boundaries were present in regions adjacent to or located between the eutectic Si particles, resulting from the higher intensity of plastic deformation in these areas. The eutectic Si particles promoted the formation of deformation zones, and these zones were associated with the formation of high-angle grain boundaries.

Post-ECAP annealing at 523 K for 2 h led to grain and/or subgrain growth in the solid solution of the alloy. The structure retained regions with low-angle subgrains located farther from the eutectic Si particles and areas with recrystallized grains near these particles, as can be seen from the electron backscatter diffraction (EBSD) analysis results presented in Figure 12.

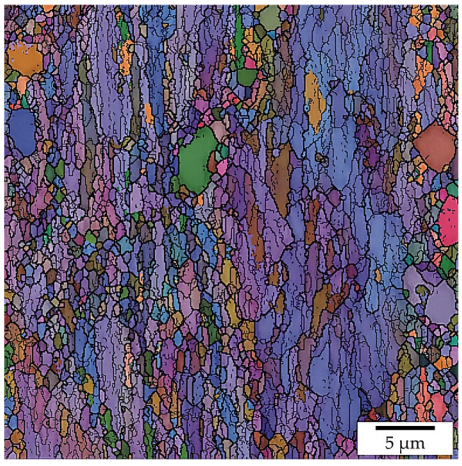


Figure 12. EBSD map of AlSi7MgCu0.5 alloy after post-ECAP annealing at 523 K for 2 h.

3.1.2. Phase Analysis of AlSi7MgCu0.5 Alloy

Phase analysis of the phases present in the alloy microstructure in the as-cast state, pre-ECAP heat-treated state, ECAP-processed state, and post-ECAP-annealed state, performed using high-energy X-ray diffraction at a synchrotron facility, confirmed the phase presence assumptions previously indicated by EDX analysis. The phase analysis confirmed the presence of major phases in the alloy structure: the Al phase corresponding to the α-solid solution and the Si phase corresponding to the eutectic particles. Figure 13 presents the diffraction pattern of the alloy in the post-ECAP annealed state, obtained during in situ diffraction measurements (results for the as-cast, pre-ECAP heat-treated, and ECAP-processed states have already been published and will be discussed in the following section). These measurements confirmed the presence of minor phases within the alloy structure. The intermetallic phases Q-$Al_4Mg_8Si_7Cu_2$ and α-$Al_{12}(Fe,Mn)_3Si$ (or possibly α-$Al_{15}(Fe,Mn)_3Si_2$) were identified, consistent with predictions from EDX analysis. Additionally, the diffraction data revealed the presence of the β-phase (Mg_2Si), which had not been detected by EDX. Based on these findings, it can be inferred that the $Al_xFe_ySi_z$ phase previously identified by EDX likely corresponds to the intermetallic α-$Al_{12}(Fe,Mn)_3Si$ or α-$Al_{15}(Fe,Mn)_3Si_2$. From the comparison of the diffraction patterns of samples measured during in situ post-ECAP annealing in the temperature range of 373–623 K, it is evident that the intensity of the Q-$Al_4Mg_8Si_7Cu_2$ phase increased with rising temperature. The diffraction data indicate that no phase dissolution occurred in the alloy structure up to 623 K. At the beginning of the diffraction patterns, additional intensity peaks are visible, which correspond to the glass seals of the furnace chamber in which the sample was placed during in situ heating and analysis.

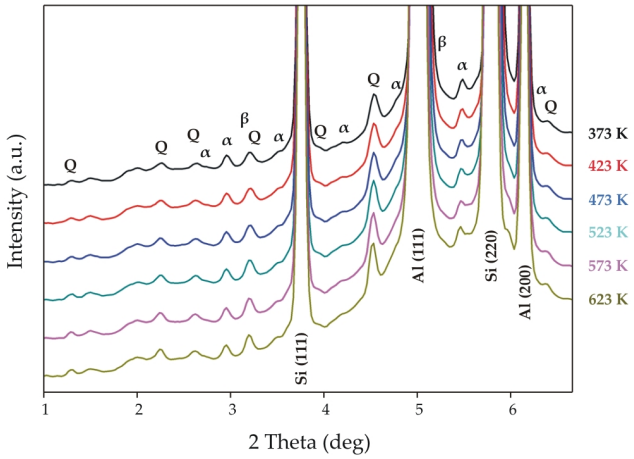


Figure 13. X-ray diffraction patterns of AlSi7MgCu0.5 alloy measured during in situ post-ECAP annealing at temperatures of 373, 423, 473, 253, 573, and 623 K.

3.2. Mechanical Properties

Processing of the as-cast alloy via pre-ECAP heat treatment, ECAP, and subsequent post-ECAP annealing resulted in modifications to its mechanical properties. The primary effect of the pre-ECAP heat treatment was an improvement in the ductility of the as-cast alloy, which was essential to enable a high degree of plastic deformation during ECAP. The ECAP technique, performed at room temperature, significantly enhanced the strength characteristics of the alloy. Subsequent post-ECAP annealing led to a gradual decrease in strength accompanied by an increase in ductility.

3.2.1. Hardness Measurements

To assess the changes in hardness of the investigated alloy states, Vickers microhardness measurements (HV0.2) were carried out. The results are summarized in Table 3. The evaluation of the microhardness in the as-cast, pre-ECAP heat-treated, and ECAP-processed states was the subject of a previous study [23], to which the present research is related. The pre-ECAP heat treatment led to a slight decrease (by 3%) in the microhardness of the as-cast AlSi7MgCu0.5 alloy. Subsequent SPD significantly increased the microhardness of the pre-ECAP-treated state by up to 58%. Post-ECAP annealing induced a reduction in microhardness values. Annealing at 373 K did not affect the microhardness of the ECAP-processed state, whereas annealing at 423 K caused a slight decrease of 0.5%, at 473 K by 8%, at 523 K by 15%, and at 573 K by 39%.

Table 3. Microhardness HV0.2 of AlSi7MgCu0.5 alloy.

Alloy State	HV0.2
As-cast [23]	72.2
Pre-ECAP heat-treated [23]	69.9
ECAP-processed [23]	110.7
Post-ECAP-annealed at 373 K	110.7
Post-ECAP-annealed at 423 K	110.1
Post-ECAP-annealed at 473 K	102.1
Post-ECAP-annealed at 523 K	94.4
Post-ECAP-annealed at 573 K	67.6

3.2.2. Tensile Testing

The strength properties and ductility characteristics of the AlSi7MgCu0.5 alloy in the as-cast state, after pre-ECAP heat treatment, after ECAP processing, and after post-ECAP annealing were determined by tensile testing at room temperature. The results of the evaluation of the 0.2% offset yield strength ($Rp_{0.2}$), ultimate tensile strength (Rm), uniform elongation (Ag), total elongation (A), and reduction in area (Z) for the analyzed AlSi7MgCu0.5 alloy are presented in Table 4. The evaluation of these characteristics in the as-cast, pre-ECAP heat-treated, and ECAP-processed states was the subject of a previous related study [23]. The as-cast state of the alloy exhibited relatively low values of both strength and ductility characteristics. Pre-ECAP heat treatment to the overaged condition led to a slight increase in yield strength from 127 MPa to 136 MPa and a decrease in ultimate tensile strength from 219 MPa to 208 MPa. Elongation increased from 10.1% to 17.1%, uniform elongation slightly decreased from 8.9% to 7.6%, and the reduction in area doubled from 14.6% to 28.2%. ECAP processing of the AlSi7MgCu0.5 alloy resulted in an increase of 135% in yield strength and 60% in ultimate tensile strength compared with the overaged state. However, this was accompanied by a slight reduction in total elongation to 14.5%, a significant decrease in uniform elongation to 1.8%, and a reduction in the reduction in area to 21.5%. Post-ECAP annealing at 373 K for 2 h caused a slight increase in both yield strength and ultimate tensile strength by nearly 10 MPa. Further increases in annealing temperature resulted in a gradual decrease in strength and a concurrent increase in ductility. Up to a temperature of 423 K, no significant changes in the mechanical properties were observed, suggesting that the alloy retained thermal stability up to this temperature. Annealing at 573 K led to a substantial decrease in strength and a corresponding increase in ductility compared with both the as-cast and overaged states. The stress–strain curves of the alloy shown in Figure 14 illustrate the comparison of the fundamental mechanical characteristics for the ECAP-processed and post-ECAP-annealed alloy states.

Table 4. Strength and ductility characteristics of AlSi7MgCu0.5 alloy.

Alloy State	$Rp_{0.2}$ [MPa]	Rm [MPa]	A [%]	Ag [%]	Z [%]
As-cast [23]	127	219	10.1	8.9	14.6
Pre-ECAP heat-treated [23]	136	208	17.1	7.6	28.2
ECAP-processed [23]	319	332	14.5	1.8	21.5
Post-ECAP-annealed at 373 K	328	340	13.4	1.5	24.0
Post-ECAP-annealed at 423 K	304	317	13.1	1.6	20.4
Post-ECAP-annealed at 473 K	282	302	14.3	2.3	25.0
Post-ECAP-annealed at 523 K	255	275	16.9	2.9	27.8
Post-ECAP-annealed at 573 K	140	200	27.0	10.0	37.6

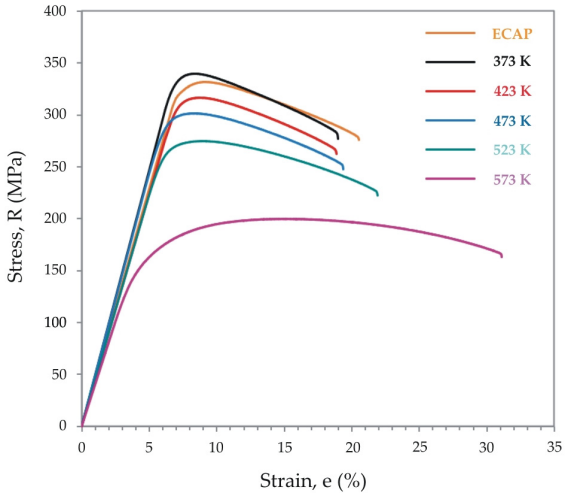


Figure 14. Stress–strain (R–e) curves of the AlSi7MgCu0.5 alloy in the ECAP-processed state and after post-ECAP annealing (373–573 K) obtained from tensile testing at room temperature.

3.2.3. Impact Toughness Testing

The impact toughness of the alloy was evaluated by Charpy impact testing in three-point bending at room temperature. The results for selected alloy states are presented in Table 5. The as-cast state exhibited not only a low level of ductility but also low values of impact toughness. Pre-ECAP heat treatment led to a significant improvement in the alloy's impact toughness. Specifically, the toughness value increased by 101% compared with the as-cast condition. Processing the alloy via the ECAP technique resulted in a decrease in impact toughness by 33%. These findings were previously reported in [23], which the present research builds upon. Post-ECAP annealing of the alloy at 523 K resulted in a 43% increase in impact toughness compared with the ECAP-processed state.

Table 5. Impact toughness of AlSi7MgCu0.5 alloy.

Alloy State	KCU [$J \cdot cm^{-2}$]
As-cast [23]	7.9
Pre-ECAP heat-treated [23]	15.9
ECAP-processed [23]	10.7
Post-ECAP-annealed at 523 K	15.3

4. Discussion

The results of the research presented in this article builds upon experiments published in [23], in which the authors investigated microstructure changes and improvements in the

mechanical properties of as-cast AlSi7MgCu0.5 alloy induced by heat treatment and the ECAP technique at room temperature.

The initial condition used for evaluating the influence of the ECAP technique on the microstructure and mechanical properties of the alloy was the as-cast state, characterized by a primary heterogeneous dendritic structure. This structure consisted of dendrites of the α-solid solution, eutectic Si particles, and intermetallic phase particles, which is typical for Al–Si–Cu–Mg alloys [14,22]. Phase analysis of the alloy structure, performed using high-energy X-ray diffraction, confirmed the presence of the major phases: Al (α-solid solution) and Si (eutectic particles). The identified minor phases included Q-$Al_4Mg_8Si_7Cu_2$, π($Al_8FeMg_3Si_6$), β(Mg_2Si), and α-$Al_{12}(Fe,Mn)_3Si$, or possibly α-$Al_{15}(Fe,Mn)_3Si_2$. The Q-$Al_4Mg_8Si_7Cu_2$ phase corresponds to the frequently observed Q-$Al_5Mg_8Si_6Cu_2$ phase, commonly found in alloys of this chemical composition [32–35]. According to the findings in [28], the average size of eutectic Si particles in the as-cast state of the AlSi7MgCu0.5 alloy was relatively small (d = 0.5 μm), while their areal number density was high (n = 21.3 × 10^4 mm^{-2}). This was achieved through Sr modification, Ti inoculation, and optimization of the cooling rate during solidification [16]. The eutectic Si particles in the as-cast structure exhibited a rod-like morphology typical for hypoeutectic modified Al–Si alloys [36]. The intermetallic phase particles present in the microstructure of the AlSi7MgCu0.5 alloy had an average size of 1.9 μm and an areal number density of 0.31 × 10^4 mm^{-2}. Intermetallic phase particles based on Fe and Mn are considered impurities in the structure of Al–Si alloys, and their increased content is known to reduce strength parameters, ductility, and toughness of these alloys [37–42]. The as-cast state was characterized by low levels of microhardness, impact toughness, elongation, and contraction due to the heterogeneous structure and unfavorable morphology of brittle intermetallic phase particles and eutectic particles consisting of rod-like eutectic Si particles in the solid solution matrix [21,22].

An effective approach to increase the plasticity of the as-cast state of the analyzed alloy prior to ECAP processing is optimized heat treatment [23]. The enhanced plasticity of the alloy enabled processing with the maximum number of passes through the ECAP die, thereby maximizing the level of its mechanical properties. An optimized overaged state of the alloy was prepared by a combination of solution annealing at 823 K for 4 h, followed by quenching and artificial aging at 573 K for 5 h. During solution annealing of the alloy, spheroidization and significant coarsening of eutectic Si particles occurred, along with the dissolution or morphological transformation of intermetallic phase particles [22,34,39]. The rod-like eutectic Si particles fragmented into smaller segments due to reduced surface tension and then spheroidized, subsequently coarsening by diffusion growth at the solution annealing temperature [21,39]. In the case of pre-ECAP heat treatment of the AlSi7MgCu0.5 alloy, the average size of eutectic Si particles increased sixfold to 3.0 μm, while their areal density decreased from 21.3 to 1.0 × 10^4 mm^{-2}. Based on the diffraction patterns obtained by synchrotron radiation for the as-cast and overaged states of the AlSi7MgCu0.5 alloy, as published in [23], it was found that solution annealing led to the dissolution of π($Al_8FeMg_3Si_6$) intermetallic phase particles and a slight increase in the volume fraction of the α-$Al_{12}(Fe,Mn)_3Si$ or α-$Al_{15}(Fe,Mn)_3Si_2$ phase, which may have occurred during either solution annealing or subsequent artificial aging. No significant change in the average size of the intermetallic particles (2.0 μm) was observed compared with the as-cast state; however, their areal density significantly decreased by ~70% to 0.09 × 10^4 mm^{-2}. A significant volume increase was recorded for the Q-$Al_4Mg_8Si_7Cu_2$ phase and a moderate increase for the β(Mg_2Si) phase compared with the as-cast state, which is also confirmed by the results reported in [34]. It can be assumed, however, that both phases dissolved during solution annealing and reprecipitated from the solid solution during artificial aging in the

form of incoherent particles [34,43,44]. Selected area electron diffraction (SAED) analysis in TEM in [23] confirmed that artificial aging led to the precipitation of incoherent particles of β(Mg_2Si), Q-$Al_4Mg_5Si_4Cu$, $Al_xFe_ySi_z$, and Si from the α-solid solution. These particles had an average size of 114 nm and an areal density of 3.5×10^6 mm^{-2}, and were uniformly distributed throughout the matrix. The interplanar spacings of the Q-$Al_4Mg_5Si_4Cu$ phase identified by SAED matched those of the Q-$Al_4Mg_8Si_7Cu_2$ phase identified by X-ray diffraction, with a deviation of only 0.001 nm; however, more precise analysis confirmed the presence of the Q-$Al_4Mg_5Si_4Cu$ phase. The $Al_xFe_ySi_z$ phase identified by SAED in TEM can be considered the α-$Al_{12}(Fe,Mn)_3Si$ or possibly α-$Al_{15}(Fe,Mn)_3Si_2$ intermetallic phase, also confirmed by X-ray diffraction. The application of the optimized heat treatment resulted in a significant increase in both impact toughness and plasticity, which was the intended goal of this processing route [22]. Processing the alloy to the overaged state increased its impact toughness by 100% (15.9 $J \cdot cm^{-2}$) and ductility by 1.7 times (17.1%) compared with the as-cast condition. Importantly, the increase in plasticity of the overaged state did not lead to a reduction in strength. The improvement in plasticity due to the pre-ECAP heat treatment was primarily achieved by eliminating the embrittling effect of the particle morphology through spheroidization of eutectic Si and the dissolution or morphological modification of intermetallic phases. The uniform precipitation of fine incoherent particles from the solid solution during artificial aging compensated for the loss of strengthening caused by the coarsening of the eutectic Si particles. As a result, the alloy exhibited nearly the same yield strength and ultimate tensile strength as in the as-cast state (variation within ~10 MPa).

An appropriate selection of SPD parameters has a very positive effect on the mechanical properties of cast aluminum alloys [10,11,14,20]. The experiments conducted in this study confirmed these findings for AlSi7MgCu0.5-type alloys and further demonstrated the importance of their optimized pre-ECAP heat treatment. Severe plastic deformation of the alloy, carried out using the ECAP technique at room temperature following heat treatment, significantly altered the character of its microstructure. The deformation induced fragmentation and redistribution of eutectic Si particles, intermetallic phases, and precipitates into a more homogeneous state. Moreover, an UFG structure of the alloy was formed, which led to increased strength and ductility, as confirmed by the findings of other authors [11,22]. Microstructural analysis revealed that the redistribution of eutectic Si particles resulted from multiple SPDs by simple shear at the ECAP die channel intersection. In cross sections of the extruded sample cut in the X and Y planes, dendritic microstructure heterogeneity was successfully eliminated. However, in the Z plane cross section, a significant heterogeneity in the arrangement of eutectic particles remained. This discrepancy arises from the deformation mechanism characteristic of route A processing [10,11]. The fragmentation of eutectic Si particles due to the high degree of imposed strain manifested in a slight decrease in their average size in the X plane (from 3.0 to 2.5 μm), accompanied by a 50% increase in their areal number density compared with the overaged state. The decrease in average particle size of intermetallic phases (from 2.0 to 1.6 μm) and the doubling of their areal number density, along with the size reduction in precipitates (from 114 to 77 nm) and the doubling of their number density compared with the overaged state, are also attributable to their fragmentation. The fragmentation of phase particles in the structure of ECAP-processed Al–Si alloys has also been reported in [11,14,16,18,22]. After ECAP processing, the alloy structure still contained minor phases such as α-$Al_{15}(Fe,Mn)_3Si_2$ or α-$Al_{12}(Fe,Mn)_3Si$, β(Mg_2Si), and Q-$Al_4Mg_8Si_7Cu_2$, similar to the overaged condition prior to ECAP. Processing of pre-ECAP heat-treated alloys using the ECAP technique resulted in the formation of an UFG matrix structure. Transmission electron microscopy revealed elongated grains or subgrains with high dislocation densities, separated primarily by

curved high-energy boundaries, which were also observed in [16]. Diffraction analysis confirmed that these grains or subgrains were separated by both low-angle and high-angle boundaries, indicating a certain degree of texture. The average subgrain width and length of the AlSi7MgCu0.5 matrix were 200 nm and 650 nm, respectively—values similar to the 230 nm width and 580 nm length measured for ECAP-processed AlSi7 alloy in [16]. According to EBSD analysis [23], the grain/subgrain sizes were non-uniform due to the presence of eutectic Si particles. The structure exhibited bands of elongated subgrains in areas more distant from these Si particles, as documented and analyzed by TEM. These were separated mostly by low-angle boundaries, consistent with selected area electron diffraction results. Equiaxed grains with high-angle boundaries were observed near or between eutectic Si particles, as also noted in ECAP-processed alloys containing eutectic Si particles in [16,18,20,22]. The average size of fine equiaxed grains in AlSi7MgCu0.5 alloy was 620 nm, corresponding to the average length of elongated subgrains in matrix regions away from eutectic Si. The matrix grains near eutectic Si particles became equiaxed due to a higher level of plastic deformation in those regions compared with more distant areas. This higher deformation intensity led to dislocation accumulation and dynamic recovery in these regions [18,21,45–47]. Thus, the submicroscopic heterogeneity in the distribution of eutectic Si particles resulted in heterogeneous matrix refinement, consisting of deformation bands with elongated subgrains and regions with equiaxed grains. EBSD analysis showed that the equiaxed grains in these regions were mostly bounded by high-angle grain boundaries, similar to findings in [18] for AlSi7Mg0.6 alloy. The application of the ECAP technique led to a significant increase in the strength of the overaged alloy. The yield strength increase was more pronounced than the ultimate tensile strength, reaching up to 135% (319 MPa). The ultimate tensile strength rose by approximately 60% (to 332 MPa) for the AlSi7MgCu0.5 alloy. The alloy's ductility and reduction of area decreased compared with the overaged state but remained higher than in the as-cast condition. The percentage of uniform plastic elongation (Ag) dropped from 7.6% to 1.8% due to strain hardening of the solid solution during ECAP [48]. The notch toughness of the overaged AlSi7MgCu0.5 alloy decreased by ~30% (to 10.7 J·cm^{-2}), yet this was still higher than in the as-cast state. The strength and ductility improvements after ECAP were due to strain hardening of the matrix, grain and/or subgrain boundary strengthening, and homogenization and fragmentation of eutectic Si, intermetallic phases, and precipitates within the solid solution, as documented in [11,16,20,49,50].

The UFG structure formed by SPD and the strain hardening of the solid solution in Al–Si alloys—along with the resulting improvement in their mechanical properties—remain stable only up to relatively low temperatures [18]. Therefore, it is crucial to identify the critical temperatures at which recovery and recrystallization of the deformed structure, or significant grain growth of the solid solution, occur, as these structural changes lead to a substantial reduction in strength. Post-ECAP annealing of the AlSi7MgCu0.5 alloy partially confirms the results presented by the authors in [18]. Within the annealing temperature range up to 573 K, no microscopically observable changes in the structure of these alloys were detected (e.g., redistribution of eutectic Si particles, intermetallic phases, and precipitates); however, significant modifications occurred at the substructural level. X-ray diffraction analysis revealed that the volume fraction of the Q-$Al_5Mg_8Si_6Cu_2$ phase increased with rising annealing temperature. As the annealing temperature increased up to 523 K, the average grain and subgrain size of the solid solution in the analyzed X plane increased from approximately 200 nm to 400 nm in width and from ~500 nm to ~950 nm in length. These results indicate that the alloy retained its UFG structure with elongated grains or subgrains under 1 μm in size up to a temperature of 523 K. Annealing at 573 K resulted in the formation of a bimodal grain size distribution in the solid solution. Equiaxed

grains with an average size of 5 μm and equilibrium grain boundaries formed near eutectic Si particles, while deformed elongated grains or subgrains with average dimensions of ~0.5 μm in width and ~1.5 μm in length were observed in regions farther from eutectic Si. Selected area electron diffraction indicated that the structure primarily consisted of grains with high-angle boundaries. This substructural transformation in the analyzed alloys was attributed to discontinuous recrystallization of the solid solution. Grain growth in areas near eutectic Si particles was driven by the higher mobility of high-angle grain boundaries present in regions subjected to greater plastic deformation intensity [20,51–53]. Based on the findings in [18], which studied post-ECAP annealing of non-heat-treatable Al–Si alloys (without Mg and Cu) processed by ECAP at room temperature, the critical stability temperature of the UFG structure was identified as 473 K. At 523 K, discontinuous recrystallization of the solid solution and the formation of a bimodal structure had already occurred. The discrepancy in results can be attributed to the presence of fine precipitate particles within the solid solution of the AlSi7MgCu0.5 alloy, which likely slow down the progress of discontinuous recrystallization and abnormal grain growth [18]. Changes in the substructure of ECAP-processed alloys during heating were naturally reflected in their mechanical properties. For the AlSi7MgCu0.5 alloy, post-ECAP annealing at 373 K led to a slight increase in yield strength and ultimate tensile strength values by approximately 10 MPa. This phenomenon can be explained by secondary precipitation hardening of the solid solution, since local deformation-induced dissolution of precipitate particles might have occurred during ECAP processing. A similar mechanism was observed in age-hardenable Al–Cu alloys, where coherent θ″-Al_2Cu and semi-coherent θ′-Al_2Cu particles reprecipitated after being dissolved during intense plastic deformation at room temperature [54,55]. Further increases in annealing temperature led to a gradual decline in strength and an increase in ductility characteristics of the AlSi7MgCu0.5 alloy. This behavior is attributed to precipitate coarsening, recovery, and partial recrystallization of the solid solution's substructure. During this process, dislocation density decreased only slightly due to dislocation annihilation, thermally activated climb, cross slip, and the replacement of the dislocation structure by newly formed discontinuously recrystallized grains [18,56]. The uniform plastic elongation (Ag) at maximum load retained similar values compared with the ECAP-processed condition up to 523 K, suggesting that the structure was not yet fully recrystallized. However, annealing at 573 K increased Ag to 10%. Evaluation of the mechanical properties of the alloy shows that they can be considered thermally stable up to 423 K. A significant drop in strength and increase in ductility to levels comparable with the overaged state occurred only after annealing at 573 K, as a result of confirmed discontinuous recrystallization and the formation of a bimodal grain structure in the solid solution [51–53].

5. Conclusions

This study focused on the thermal stability of the ultra-fine-grained (UFG) structure and the mechanical properties of the AlSi7MgCu0.5 alloy processed by equal channel angular pressing (ECAP) at room temperature. The following conclusions can be drawn:

(1) Post-ECAP annealing was employed to evaluate the thermal stability of the strain- and precipitation-hardened UFG structure and the resulting mechanical properties. With increasing annealing temperature, a progressive growth in the average grain and/or subgrain size of the solid solution occurred primarily due to recovery and recrystallization processes. The UFG structure remained stable up to 523 K, with grain or subgrain sizes maintained below 1 μm. Annealing at 573 K triggered discontinuous recrystallization, resulting in a bimodal grain structure: near eutectic Si particles, equiaxed grains formed (~5 μm), while more distant regions retained

elongated deformed grains or subgrains (~0.5 μm width, ~1.5 μm length). Furthermore, the volume fraction of the Q-$Al_5Mg_8Si_6Cu_2$ phase increased gradually with annealing temperature.

(2) Substructural transformations induced by annealing led to corresponding changes in mechanical behavior. As the annealing temperature increased, the alloy exhibited a gradual reduction in strength and an increase in ductility, consistent with ongoing recovery and recrystallization. An exception was observed at 373 K, where a slight increase (~10 MPa) in yield strength ($Rp_{0.2}$) and ultimate tensile strength (Rm) was recorded, likely due to additional precipitation hardening. Since no significant deterioration in mechanical properties was observed up to 423 K, the ECAP-processed alloy can be considered thermally stable up to this temperature. Discontinuous recrystallization at 573 K led to a marked decline in strength and a recovery of ductility to levels comparable with the pre-ECAP-treated state.

Author Contributions: Conceptualization, M.M.; methodology, M.M., M.F. and O.M.; software, M.M. and O.M.; validation, M.M., M.F., O.M., M.V. and K.G.; formal analysis, M.M. and M.F.; investigation, M.M., M.F., O.M., M.V. and K.G.; resources, M.M.; data curation, M.M. and M.F.; writing—original draft preparation, M.M.; writing—review and editing, M.M. and M.F.; visualization, M.M.; supervision, M.M. and M.F.; project administration, K.G.; funding acquisition, M.F. All authors have read and agreed to the published version of the manuscript.

Funding: This work was supported by the Slovak Research and Development Agency under Contract No. APVV-23-0030, VEGA Project No. 1/0122/25, and KEGA Project No. 011TUKE-4/2025.

Data Availability Statement: The data presented in this study are available in the article.

Acknowledgments: The authors thank Deutsches Elektronen-Synchrotron (DESY) for the provision of the storage ring-based X-ray radiation source PETRA III in using the undulator beamline P21.1.

Conflicts of Interest: The authors declare no conflicts of interest.

Abbreviations

The following abbreviations are used in this manuscript:

EBSD	electron backscatter diffraction
ECAP	equal channel angular pressing
EDX	energy dispersive X-ray
LM	light microscopy
SAED	selected area electron diffraction
SE	secondary electron
SEM	scanning electron microscopy
SPD	severe plastic deformation
TEM	transmission electron microscopy
UFG	ultra-fine-grained
XRD	X-ray diffraction

References

1. Zhou, P.; Wang, D.; Nagaumi, H.; Wang, R.; Zhang, X.; Li, X.; Zhang, H.; Zhang, B. Microstructural Evolution and Mechanical Properties of Al-Si-Mg-Cu Cast Alloys with Different Cu Contents. *Metals* **2023**, *13*, 98. [CrossRef]
2. Choi, S.; Kim, Y.; Kim, Y.; Kang, C. Effects of alloying elements on mechanical and thermal characteristics of Al-6wt-%Si-0.4wt-%Mg–(Cu) foundry alloys. *Mater. Sci. Technol.* **2019**, *35*, 1365–1371. [CrossRef]
3. Chen, B.; Dong, L.; Hu, B.; Liu, Z. The Effect of Cu Addition on the Precipitation Sequence in the Al-Si-Mg-Cr Alloy. *Materials* **2022**, *15*, 8221. [CrossRef]
4. Segal, V.M.; Reznikov, V.I.; Drobyshevskiy, A.E.; Kopylov, V.I. Plastic Working of Metals by Simple Shear. *Metally* **1981**, *1*, 99–105.
5. Hall, E.O. The deformation and ageing of mild steel: III Discussion of results. *Proc. Phys. Soc. Lond. B* **1951**, *64*, 747–753. [CrossRef]

6. Petch, N.J. The cleavage strength of polycrystals. *J. Iron Steel Inst.* **1953**, *174*, 25–28.
7. Rahmawaty, R.; Dharma, S.; Razak, A.; Sarjianto, S.; Bahri, N.; Sutrisno, J.; Suherman, S.; Abdullah, I.; Silalahi, A.R.S. The Effect of Process Route on the Mechanical Properties and Microstructure Aluminum Al-Si-Cu-Mg-Mn Alloys. *Defect Diffus. Forum* **2020**, *402*, 67–72. [CrossRef]
8. Furukawa, M.; Iwahashi, Y.; Horita, Z.; Nemoto, M.; Langdon, T.G. The shearing characteristics associated with equal-channel angular pressing. *Mater. Sci. Eng. A* **1998**, *257*, 328–332. [CrossRef]
9. Wang, J.; Iwahashi, Y.; Horita, Z.; Furukawa, M.; Nemoto, M.; Valiev, R.Z.; Langdon, T.G. An investigation of microstructural stability in an Al-Mg alloy with submicrometer grain size. *Acta Mater.* **1996**, *44*, 2973–2982. [CrossRef]
10. Garcia-Infanta, J.M.; Swaminathan, S.; Zhilyaev, A.P.; Carreño, F.; Ruano, O.A.; McNelley, T.R. Microstructural development during equal channel angular pressing of hypo-eutectic Al–Si casting alloy by different processing routes. *Mater. Sci. Eng. A* **2008**, *485*, 160–175. [CrossRef]
11. Gutierrez Urrutia, I.; Muñoz Morris, M.A.; Morris, D.G. Effects of ECAP processing on discontinuous dynamic recrystallization. *Acta Mater.* **2007**, *55*, 1319–1330. [CrossRef]
12. Ma, A.; Takagi, M.; Saito, N.; Iwata, H.; Nishida, Y.; Suzuki, K.; Shigematsu, I. Tensile properties of an Al–11 mass%Si alloy at elevated temperatures processed by rotary-die equal-channel angular pressing. *Mater. Sci. Eng. A* **2005**, *408*, 147–153. [CrossRef]
13. Ma, A.; Suzuki, K.; Nishida, Y.; Saito, N.; Shigematsu, I.; Takagi, M.; Iwata, H.; Watazu, A.; Imura, T. Impact toughness of an ultrafine-grained Al–11mass%Si alloy processed by rotary-die equal-channel angular pressing. *Acta Mater.* **2005**, *53*, 211–220. [CrossRef]
14. Ma, A.; Saito, N.; Takagi, M.; Nishida, Y.; Iwata, H.; Suzuki, K.; Shigematsu, I.; Watazu, A. Effect of severe plastic deformation on tensile properties of a cast Al–11 mass% Si alloy. *Mater. Sci. Eng. A* **2005**, *395*, 70–76. [CrossRef]
15. Kim, J.C.; Nishida, Y.; Arima, H.; Ando, T. Microstructure of Al–Si–Mg alloy processed by rotary-die equal channel angular pressing. *Mater. Lett.* **2003**, *57*, 1689–1695. [CrossRef]
16. Gutierrez Urrutia, I.; Muñoz Morris, M.A.; Puertas, I.; Luis, C.; Morris, D.G. Influence of processing temperature and die angle on the grain microstructure produced by severe deformation of an Al–7% Si alloy. *Mater. Sci. Eng. A* **2008**, *475*, 268–278. [CrossRef]
17. Cepeda Jiménez, C.M.; Garcia Infanta, J.M.; Zhilyaev, A.P.; Ruano, O.A.; Carreño, F. Influence of the supersaturated silicon solid solution concentration on the effectiveness of severe plastic deformation processing in Al–7 wt.% Si casting alloy. *Mater. Sci. Eng. A* **2011**, *528*, 7938–7947. [CrossRef]
18. Moradi, M.; Nili Ahmadabadi, M.; Heidarian, B. Improvement of mechanical properties of AL (A356) cast alloy processed by ECAP with different heat treatments. *Int. J. Mater. Forming* **2009**, *2*, 85–88. [CrossRef]
19. Szczygiel, P.; Roven, H.J.; Reiso, O. On the effect of severe plastic deformation on recycled experimental aluminium alloys: Nanostructures, particle break up and properties. *Mater. Sci. Eng. A* **2005**, *410–411*, 261–264. [CrossRef]
20. Garcia-Infanta, J.M.; Zhilyaev, A.P.; Capeda-Jiménez, C.M.; Ruano, O.A.; Careno, F. Effect of the deformation path on the ductility of a hypoeutectic Al–Si casting alloy subjected to equal-channel angular pressing by routes A, B_A, B_C and C. *Scr. Mater.* **2008**, *58*, 138–141. [CrossRef]
21. Swaminathan, S.; Garcia-Infanta, J.M.; McNelley, T.R.; Ruano, O.A.; Carreño, F. Severe plastic deformation of an as-cast hypoeutectic Al–Si alloy. *J. Mater. Sci.* **2008**, *43*, 7501–7506. [CrossRef]
22. Nishida, Y.; Arima, H.; Kim, J.C.; Ando, T. Rotary-die equal-channel angular pressing of an Al–7 mass% Si–0.35 mass% Mg alloy. *Scr. Mater.* **2001**, *45*, 261–266. [CrossRef]
23. Matvija, M.; Fujda, M.; Milkovič, O.; Vojtko, M.; Kočiško, R.; Glogovský, M. Microstructure Changes and Improvement in the Mechanical Properties of As-Cast AlSi7MgCu0.5 Alloy Induced by the Heat Treatment and ECAP Technique at Room Temperature. *Adv. Mater. Sci. Eng.* **2018**, *2018*, 5697986. [CrossRef]
24. Dippel, A.-C.; Liermann, H.-P.; Delitz, J.T.; Walter, P.; Schulte Schrepping, H.; Seeck, O.H.; Franz, H. Beamline P02.1 at PETRA III for high resolution and high energy powder diffraction. *J. Synchrotron Radiat.* **2015**, *22*, 675–687. [CrossRef]
25. Franz, H.; Leupold, O.; Rohlsberger, R.; Roth, S.; Seeck, O.; Spengler, J.; Strempfer, J.; Tischer, M.; Viefhaus, J.; Weckert, E.; et al. Technical Report: PETRA III: DESY's New High Brilliance Third Generation Synchrotron Radiation Source. *Synchrotron Radiat. News* **2006**, *19*, 25–29. [CrossRef]
26. Skinner, L.B.; Benmore, C.J.; Parise, J.B. Area detector corrections for high quality synchrotron X ray structure factor measurements. *Nucl. Instrum. Methods Phys. Res. A* **2012**, *662*, 61–70. [CrossRef]
27. Bednarcik, J.; Gamcova, J.; Liermann, H.P. New Heating/Cooling Stage Available to Users at P02.1. In *DESY Annual Report 2012*; DESY: Hamburg, Germany, 2012.
28. Hammersley, A.P.; Svensson, S.O.; Hanfland, M.; Fitch, A.N.; Hausermann, D. Two dimensional detector software: From real detector to idealised image or two theta scan. *High Press. Res.* **1996**, *14*, 235–248. [CrossRef]
29. *ISO 6507-1:2023*; Metallic Materials—Vickers Hardness Test. Part 1: Test Method. International Organization for Standardization: Geneva, Switzerland, 2023.

30. *ISO 6892-1:2019*; Metallic Materials—Tensile Testing. Part 1: Method of Test at Room Temperature. International Organization for Standardization: Geneva, Switzerland, 2019.
31. *ISO 148-1:2016*; Metallic Materials—Charpy Pendulum Impact Test. Part 1: Test Method. International Organization for Standardization: Geneva, Switzerland, 2016.
32. Phragmen, G.J. The coarsening behavior of strengthening particles in an Al–Cu–Mg–Ag alloy during creep. *J. Inst. Met.* **1950**, *77*, 489–552. [CrossRef]
33. Mondolfo, L.F. *Aluminum Alloys: Structure and Properties*; Butterworths: London, UK, 1976; pp. 806–841; ISBN 0 408 10827 6. [CrossRef]
34. Farkoosh, A.R.; Javidani, M.; Hoseini, M.; Larouche, D.; Pekguleryuz, M. Phase formation in as-solidified and heat-treated Al–Si–Cu–Mg–Ni alloys: Thermodynamic assessment and experimental investigation for alloy design. *J. Alloys Compd.* **2013**, *551*, 596–606. [CrossRef]
35. Unterreiter, G.; Ludwig, A.; Wu, M. Numerical microstructure prediction for an aluminium casting and its experimental validation. *China Foundry* **2011**, *8*, 331–336.
36. Nafisi, S.; Ghomashchi, R.; Vali, H. Eutectic nucleation in hypoeutectic Al-Si alloys. *Mater. Charact.* **2008**, *59*, 1466–1473. [CrossRef]
37. Wang, L.; Makhlouf, M.; Apelian, D. Aluminium die casting alloys: Alloy composition, microstructure, and properties-performance relationships. *Int. Mater. Rev.* **1995**, *40*, 221–238. [CrossRef]
38. Mohamed, A.M.A.; Samuel, F.H. Review on the Heat Treatment of Al Si Cu/Mg Casting Alloys. In *Heat Treatment: Conventional and Novel Applications*; Czerwinski, F., Ed.; InTech: Rijeka, Croatia, 2012; pp. 55–72; ISBN 978-953-51-0768-2. [CrossRef]
39. Sjölander, E.; Seifeddine, S. The heat treatment of Al–Si–Cu–Mg casting alloys. *J. Mater. Process. Technol.* **2010**, *210*, 1249–1259. [CrossRef]
40. Kearney, A.L. Properties of Cast Aluminum Alloys. In *ASM Handbook: Properties and Selection: Nonferrous Alloys and Special Purpose Materials*; ASM International Handbook Committee, Ed.; ASM International: Cleveland, OH, USA, 1990; Volume 2, pp. 569–666; ISBN 978-0-87170-378-1. [CrossRef]
41. Colás, R.; Velasco, E.; Valtierra, S. Castings. In *Handbook of Aluminum: Physical Metallurgy and Processes*; Totten, G.E., Mackenzie, D.C., Eds.; Taylor & Francis Group: Boca Raton, FL, USA, 2003; Volume 1, pp. 591–641; ISBN 978-0-20391-259-1. [CrossRef]
42. Tillová, E.; Panušková, M. Effect of solution treatment on intermetallic phases morphology in AlSi9Cu3 cast alloy. *Metalurgija* **2008**, *47*, 207–210.
43. Wang, G.; Sun, Q.; Feng, L.; Hui, L.; Jing, C. Influence of Cu content on ageing behavior of AlSiMgCu cast alloys. *Mater. Des.* **2007**, *28*, 1001–1005. [CrossRef]
44. Gupta, A.K.; Jena, A.K.; Chaturvedi, M.C. Insoluble phase in Al–1·52Cu–0·75Mg alloys containing silicon. *Mater. Sci. Technol.* **1987**, *3*, 1012–1018. [CrossRef]
45. Dennis, J.; Bate, P.S.; Humphreys, F.J. Abnormal grain growth in Al–3.5Cu. *Acta Mater.* **2009**, *57*, 4539–4547. [CrossRef]
46. Rofman, O.V.; BATE, P.S. Dynamic grain growth and particle coarsening in Al–3.5Cu. *Acta Mater.* **2010**, *58*, 2527–2534. [CrossRef]
47. Fleck, N.A.; Muller, G.M.; Ashby, M.F.; Hutchinson, J.W. Strain gradient plasticity: Theory and experiment. *Acta Metall. Mater.* **1994**, *42*, 475–487. [CrossRef]
48. Fujda, M.; Matvija, M.; Kvačkaj, T.; Milkovič, O.; Zubko, P.; Nagyová, K. Structure and properties of AlMgSi alloys after ECAP and post-ECAP ageing. *Mater. Technol.* **2012**, *46*, 465–469.
49. Hansen, N. Boundary Strengthening over Five Length Scales. *Adv. Eng. Mater.* **2005**, *7*, 815–821. [CrossRef]
50. Morris, D.G.; Gutierrez-Urrutia, I.; Munoz-Morris, M.A. Analysis of strengthening mechanisms in a severely-plastically-deformed Al–Mg–Si alloy with submicron grain size. *J. Mater. Sci.* **2007**, *42*, 1439–1443. [CrossRef]
51. Mao, W. Recrystallization and Grain Growth. In *Handbook of Aluminum: Physical Metallurgy and Processes*; Totten, G.E., Mackenzie, D.S., Eds.; Taylor & Francis Group: Boca Raton, FL, USA, 2003; Volume 1, pp. 211–258; ISBN 978-0-20391-259-1. [CrossRef]
52. Humphreys, F.J.; Hatherly, M. Grain Growth Following Recrystallization. In *Recrystallization and Related Annealing Phenomena*, 2nd ed.; Humphreys, F.J., Hatherly, M., Eds.; Elsevier: Oxford, UK, 2004; pp. 333–378; ISBN 0 08 041884-8.
53. Jazaeri, H.; Humphreys, F.J. The transition from discontinuous to continuous recrystallization in some aluminium alloys: I—the deformed state. *Acta Mater.* **2004**, *52*, 3251–3262. [CrossRef]
54. Huang, W.; Liu, Z.; Lin, M.; Zhou, X.; Zhao, L.; Ning, A.; Zeng, S. Reprecipitation behavior in Al–Cu binary alloy after severe plastic deformation-induced dissolution of θ′ particles. *Mater. Sci. Eng. A* **2012**, *546*, 26–33. [CrossRef]
55. Huang, W.; Liu, Z.; Xia, L.; Xia, P.; Zeng, S. Severe plastic deformation-induced dissolution of θ″ particles in Al–Cu binary alloy and subsequent nature aging behavior. *Mater. Sci. Eng. A* **2012**, *556*, 801–806. [CrossRef]
56. Furu, T.; Marthinsen, K.; Nes, E. Modelling recrystallisation. *Mater. Sci. Technol.* **1990**, *6*, 1093–1102. [CrossRef]

Disclaimer/Publisher's Note: The statements, opinions and data contained in all publications are solely those of the individual author(s) and contributor(s) and not of MDPI and/or the editor(s). MDPI and/or the editor(s) disclaim responsibility for any injury to people or property resulting from any ideas, methods, instructions or products referred to in the content.